Electronic Supplementary Material (ESI) for Journal of Materials Chemistry A.

Supporting Information

Multi-high valence state metal doping in NiFe hydroxide toward superior oxygen evolution reaction activity

Fitri Nur Indah Sari[1], Gally Frenel[1], Alex Chinghuan Lee[2], Yan-Jia Huang[1], Yen-Hsun Su[1], Jyh-Ming Ting[1,2*]

[1]Department of Materials Science and Engineering

[2]Hierarchical Green-Energy Materials (Hi-GEM) Research Center

National Cheng Kung University, Tainan, Taiwan

*E-mail: jting@mail.ncku.edu.tw

Table S1. Experimental matrix of hydroxide catalysts. All salt precursors have the same concentration of 0.01M.

Sample ID	$FeCl_3$ (mL)	VCl_3 (mL)	$TiCl_3$ (mL)	$Co(NO_3)_2{\cdot}6H_2O$ (mL)	$Cr(NO_3)_3{\cdot}9H_2O$ (mL)
FN	40				
FNV	40	20			
FNVTi	40	20	2		
FNVTiCo	40	20	2	2	
FNVTiCr	40	20	2		2

Information SI. Determination of Ag/AgCl reference electrode and conversion into reference hydrogen electrode (RHE)

The calibration of Ag/AgCl reference electrode was performed under linear sweep voltammetry (LSV) at 0.5 mV s^{-1} in H_2-saturated 1M KOH electrolyte to obtain the thermodynamic potential of the hydrogen electrode reaction.[1, 2] The potentials at which the current crosses zero was taken to be the thermodynamic potential for the hydrogen electrode reactions. The zero-current point was determined to be -1.01V, as shown in Figure SI. Therefore, the $E_{RHE} = E_{Ag/AgCl} + 1.01$ V.

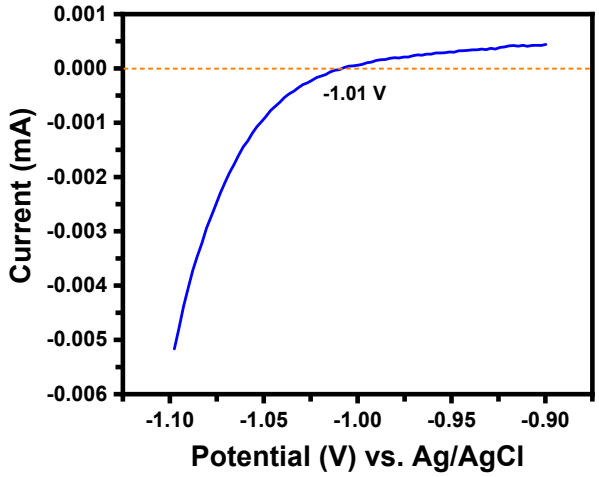

Figure SI. LSV plot of Ag/AgCl reference electrode calibration.

Information SII. Preparation of RuO_2 and Pt/C electrodes

RuO_2 and Pt/C electrodes were prepared using the same approach. A slurry containing 5 mg of as-received RuO_2 (Alfa Aesar, 99.9%) or Pt/C (Alfa Aesar, 20%), 50 μL of Nafion (5wt%), 150 μL of ethanol, and 350 μL of deionized water was first prepared. The slurry was then ultrasonicated for 30 min to obtain a homogeneous dispersion. After that, 150 μL of the slurry was dropped cast onto HCl-treated Ni foam, following by drying at 70°C for 1 h.

Information SIII Growth process of FNVTiCr hydroxide on Ni foam

FNVTiCr hydroxide was grown on Ni foam substrate using a corrosion reaction method at room temperature,[3, 4] as illustrated in Figure SII. The Ni foam acted as both a substrate and the Ni source. First, the Ni foam substrate was immersed into a $FeCl_3$ solution (0.01M and pH of 2.95). Fe^{3+} in the $FeCl_3$ solution functioned as the Fe source and oxidant for Ni oxidation.[4] The role of the Cl^- was to oxidize or corrodes the Ni foam too.[3, 4] In other words, Ni foam was corroded by both Fe^{3+} and Cl^- to become Ni^{2+} (Reaction 1). On the other hand, oxygen reduction occurred to form OH^- (Reaction 2).[3] The oxygen came from the air or those in the electrolyte. The formed OH^- then reacted with the Ni^{2+} and Fe^{3+}, giving FeNi hydroxide grown on the Ni foam surface (Reaction 3). Afterward, VCl_3, $TiCl_3$, and $Cr(NO_3)_3$ precursor solutions were then added into the Ni foam-containing $FeCl_3$ solution. This allowed the V^{3+}, Ti^{3+}, and Cr^{3+} cations to diffuse into FeNi hydroxide, forming multi-metal hydroxide (Reaction 4).

Reaction 1: $Ni\ (Fe^{3+}\text{ and }Cl^-\text{ corrosion}) \rightarrow Ni^{2+} + 2e^-$

Reaction 2: $1/2O_2 + H_2O + 2e^- \rightarrow 2OH^-$

Reaction 3: $Ni^{2+} + Fe^{k+} + (2+k)OH^- \rightarrow FeNi(OH)$

Reaction 4: $FeNi(OH)_{2+k} + V^{l+} + Ti^{m+} + Cr^{n+} + (l+m+n)OH^- \rightarrow FeNiVTiCr(OH)_{2+k+l+m+n}$

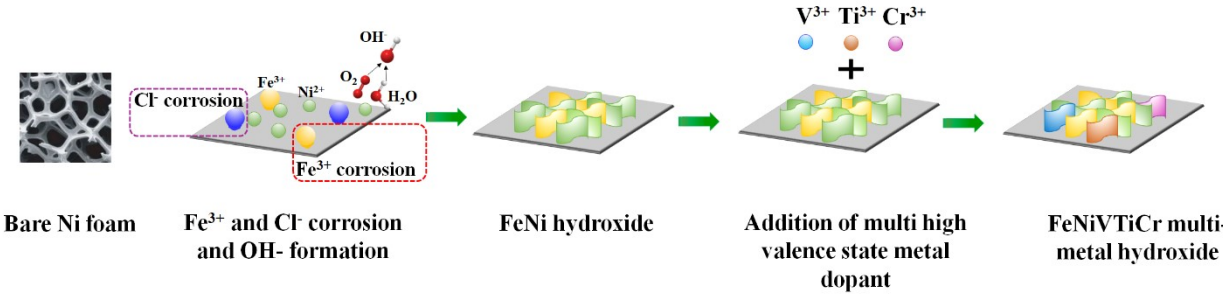

Figure SII. Schematic of the formation of multi-metal hydroxide on Ni foam substrate

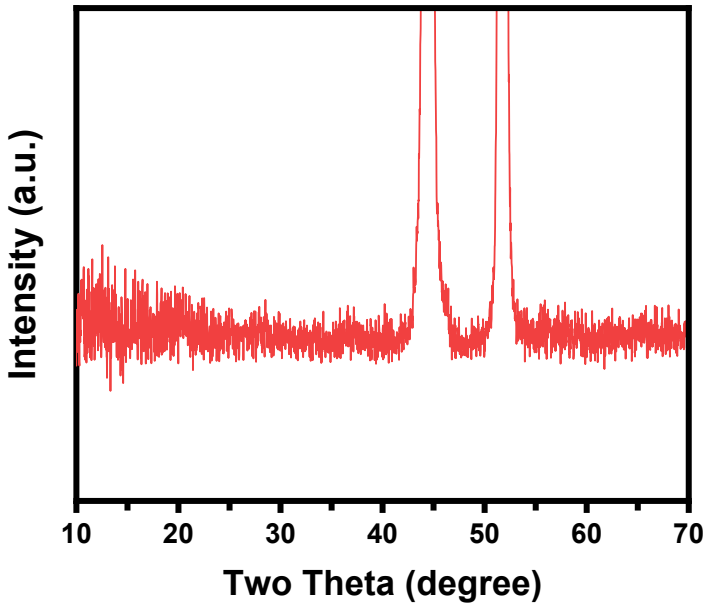

Figure S1. XRD pattern of FNVTiCr.

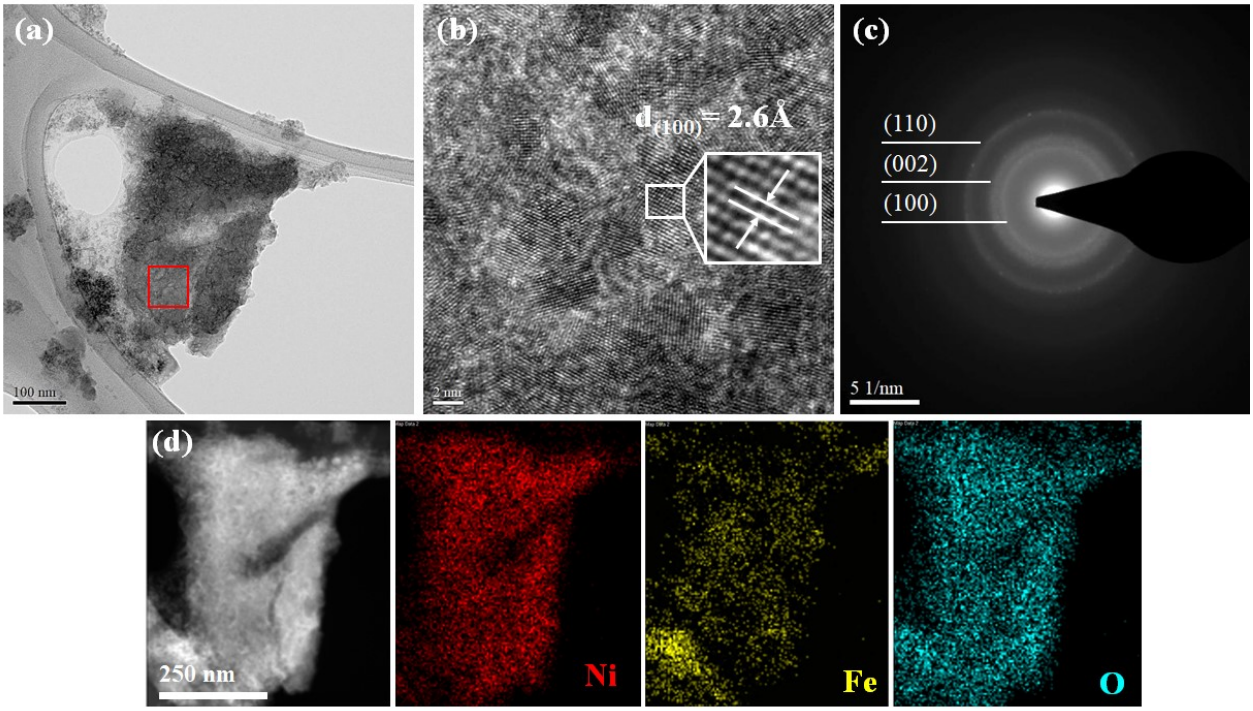

Figure S2. (a) TEM image of FN. (b) HR-TEM and (c) SAED images of the red rectangle in (a).

(d) HAADF and STEM-EDS mappings of FN.

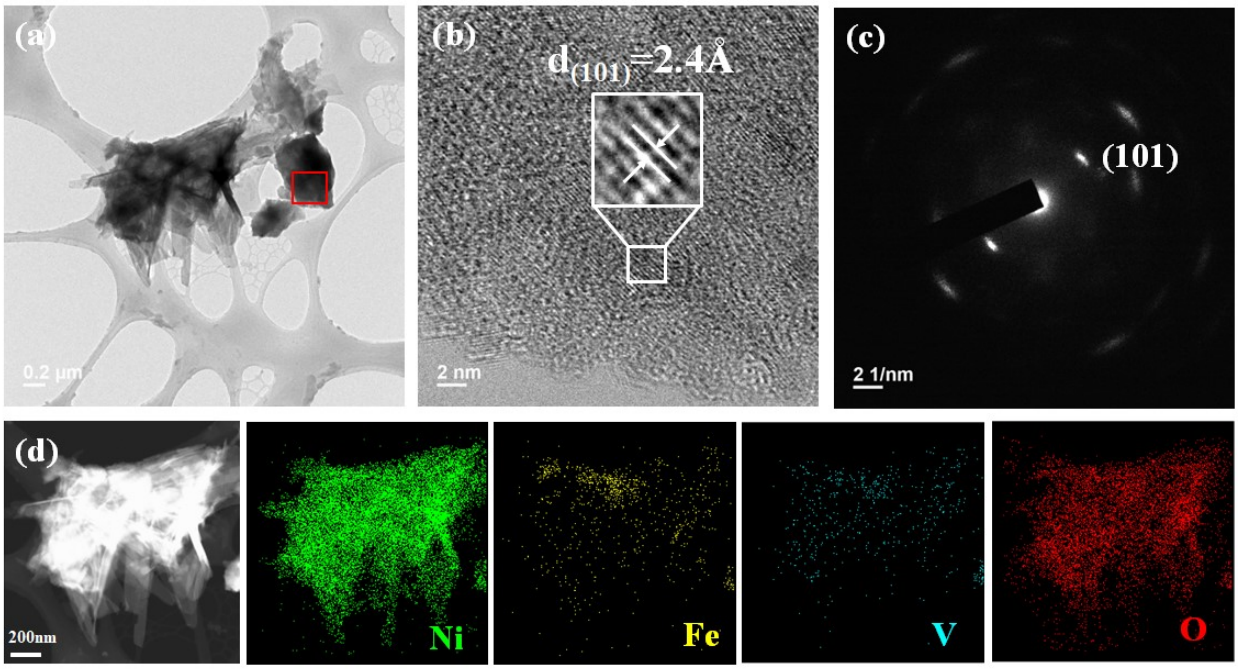

Figure S3. (a) TEM image of FNV. (b) HR-TEM and (c) SAED images of the red rectangle in (a). (d) HAADF and STEM-EDS mappings of FNV.

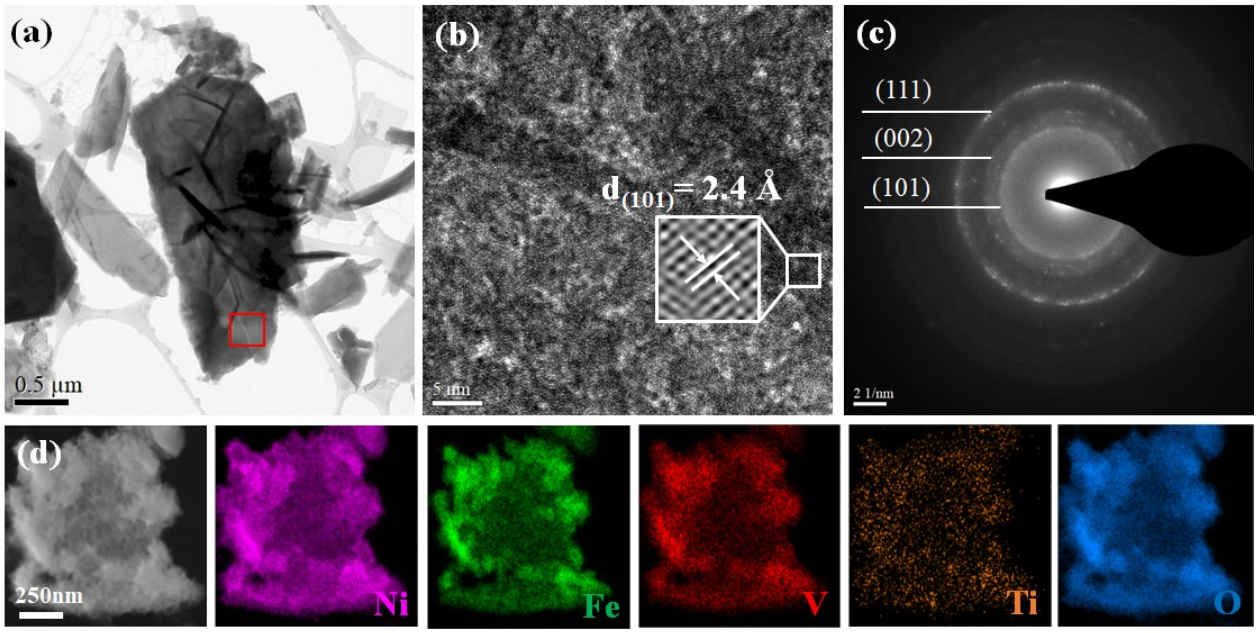

Figure S4. (a) TEM image of FNVTi. (b) HR-TEM and (c) SAED images of the red rectangle in (a). (d) HAADF and STEM-EDS mappings of FNVTi.

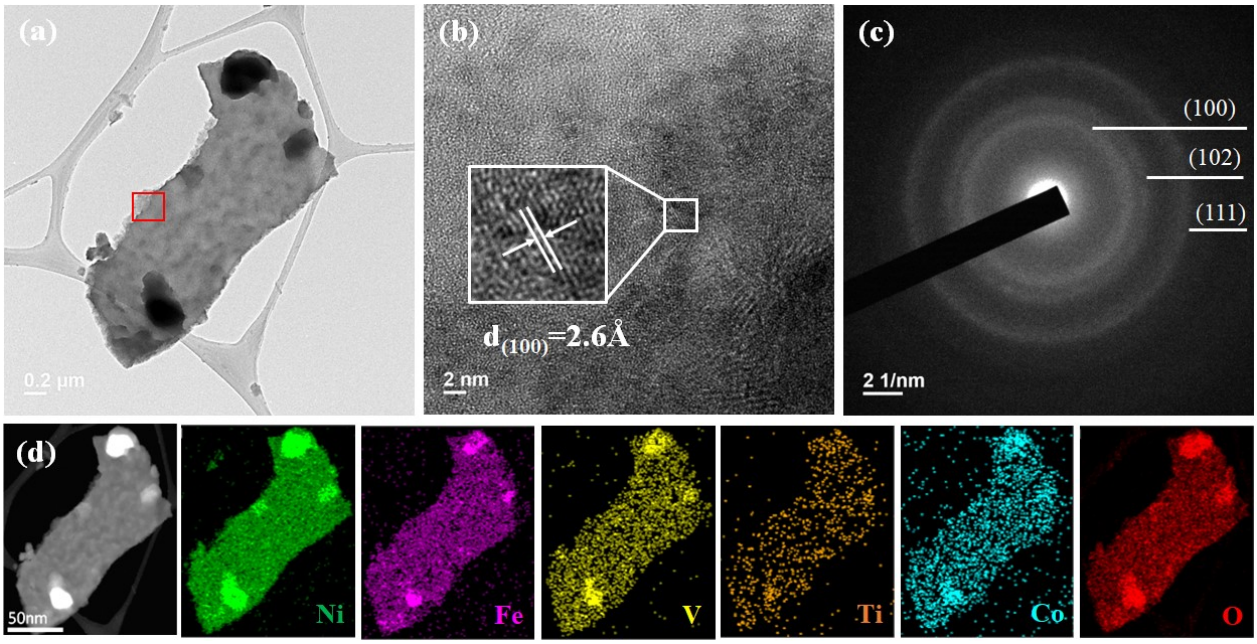

Figure S5. (a) TEM image of FNVTiCo. (b) HR-TEM and (c) SAED images of the red rectangle in (a). (d) HAADF and STEM-EDS mappings of FNVTiCo.

Table S2. Element concentration (at. %) obtained from EDS.

Sample	Ni	Fe	V	Ti	Cr	Co
FN	79.8	20.2				
FNV	63.6	27.4	9.0			
FNVTi	65.3	25.1	8.4	1.3		
FNVTiCo	67.2	20.7	7.5	0.9		3.7
FNVTiCr	71.5	18.8	7.9	1.2	0.6	

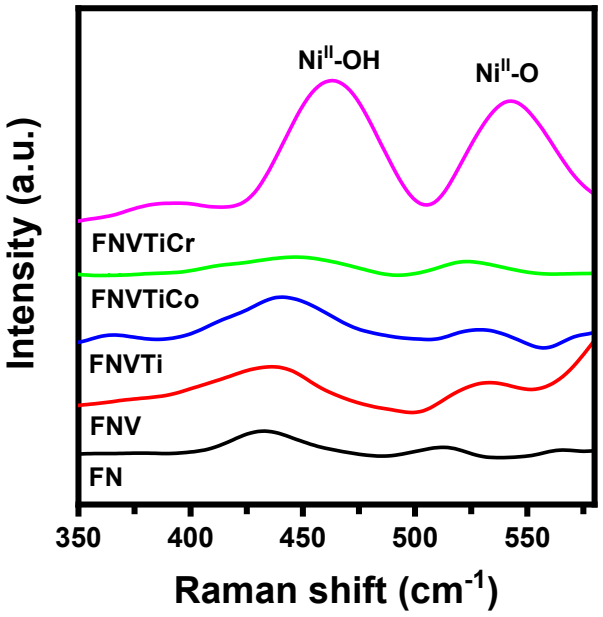

Figure S6. Enlarged Raman spectra of Figure 2e in between 350 and 580 cm^{-1}.

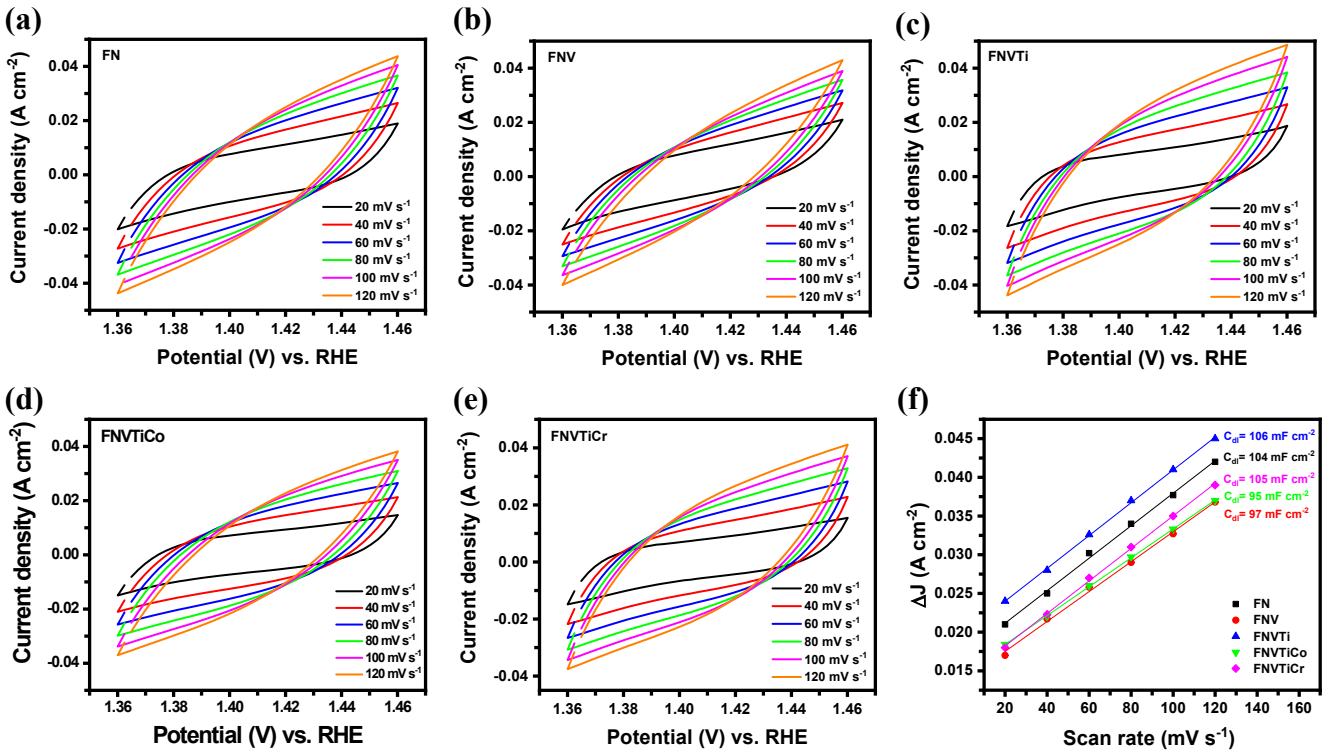

Figure S7. CV curves of (a) FN, (b) FNV, (c) FNVTi, (d) FNVTiCo, and (e) FNVTiCr. (f) The resulting C_{dl} plots.

Table S3. ECSAs and ECSA normalized overpotentials (η_{ESCA}) of the obtained hydroxides.

Sample	**ECSA (cm^2)**	**η_{ESCA} (mV) at 0.1 mA cm^{-2}**
FN	2,600	309
FNV	2,425	293
FNVTi	2,650	273
FNVTiCo	2,375	282
FNVTiCr	2,625	251

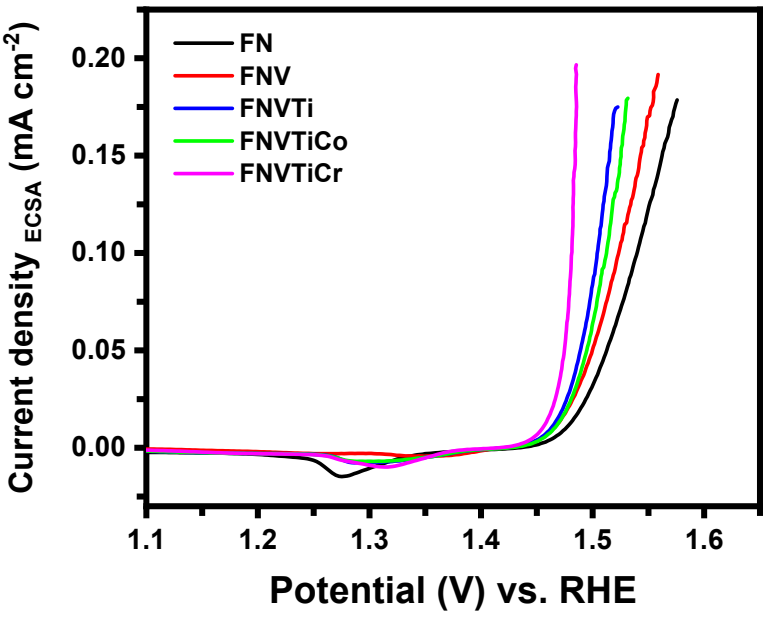

Figure S8. LSV curves normalized to the ECSA.

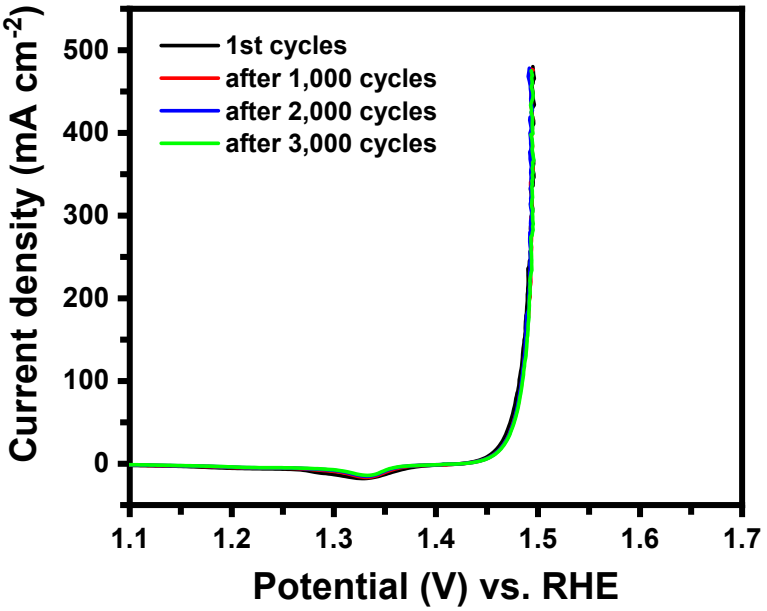

Figure S9. LSV curves of the FNVTiCr obtained after CV cycle stability.

Table S4. The comparison of the FNVCrTi hydroxide with reported NiFe-based electrocatalyst.

Catalyst	Fabrication	Substrate	η_{100} (mV)	Tafel slope (mV dec^{-1})	Stability (h)	Refs.
NiFe LDH/NiTe	Two step hydrothermal	Ni foam	270	51.04	30	[5]
P-FeNiO/CNS	Polymerization and thermal annealing under the N_2, followed by phosphorization	Glassy carbon	300	52.2	20	[6]
G-Ni0.5Fe0.5	Two-step sol–gel and carbothermal	Glassy carbon	410	43	10	[7]
hcp-NiFe@NC	Two-step solvothermal and annealing	Carbon cloth	263	41	35	[8]
Ni_xFe_{1-x}– AHNAs	Chemical deposition method with the assistance of uniform magnetic field	Ni foam	230	34.7	120	[9]
Fe-enriched $Ni(Fe)O_xH_y$	Electrodeposition followed by molten salt method	Ni foam	250	31	50	[10]
Fe_xNi_{1-x} alloy fiber paper	Chemical deposition and annealing	fiber paper	287	67	80	[11]
FeOOH-NiOOH	Corrosion reaction method	Ni foam	260	38	-	[12]
$FeNi_3$ and NiCu alloys	Solvothermal followed by two-step annealing	Ni foam	250	34	200	[13]
MoFe: $Ni(OH)_2$/NiOOH	Hydrothermal	Ni foam	280	47	50	[14]
FeNiCoCrMn-high entropy glycerate (HEG)	Solvothermal	Ni foam	270	40	36	[15]
$FeNiCoCrMnS_2$	Two-step solvothermal	Ni foam	246	39.1	55	[16]
CrMnFeCoNiTi Zn HEG	Solvothermal	Ni foam	260	42.3	60	[17]
MgFeCoNi $Cu(O)_2$ spinel oxide	Co-precipitation and annealing	Ni foam	350	40	25	[18]
FeCoNiMn (oxy)hydroxide	Electrodeposition	Ni foam	290	69	200	[19]
FNVTiCr hydroxide	Room temperature corrosion reaction method	Ni foam	240	29	70	This work

Table S5. Ni 2p spectra analysis.

Sample ID	Ni^{2+} (%)	Ni^{3+} (%)
FN	78.3	21.7
FNV	74.5	25.5
FNVTi	72.4	27.6
FNVTiCo	73.1	26.9
FNVTiCr	70.4	29.6

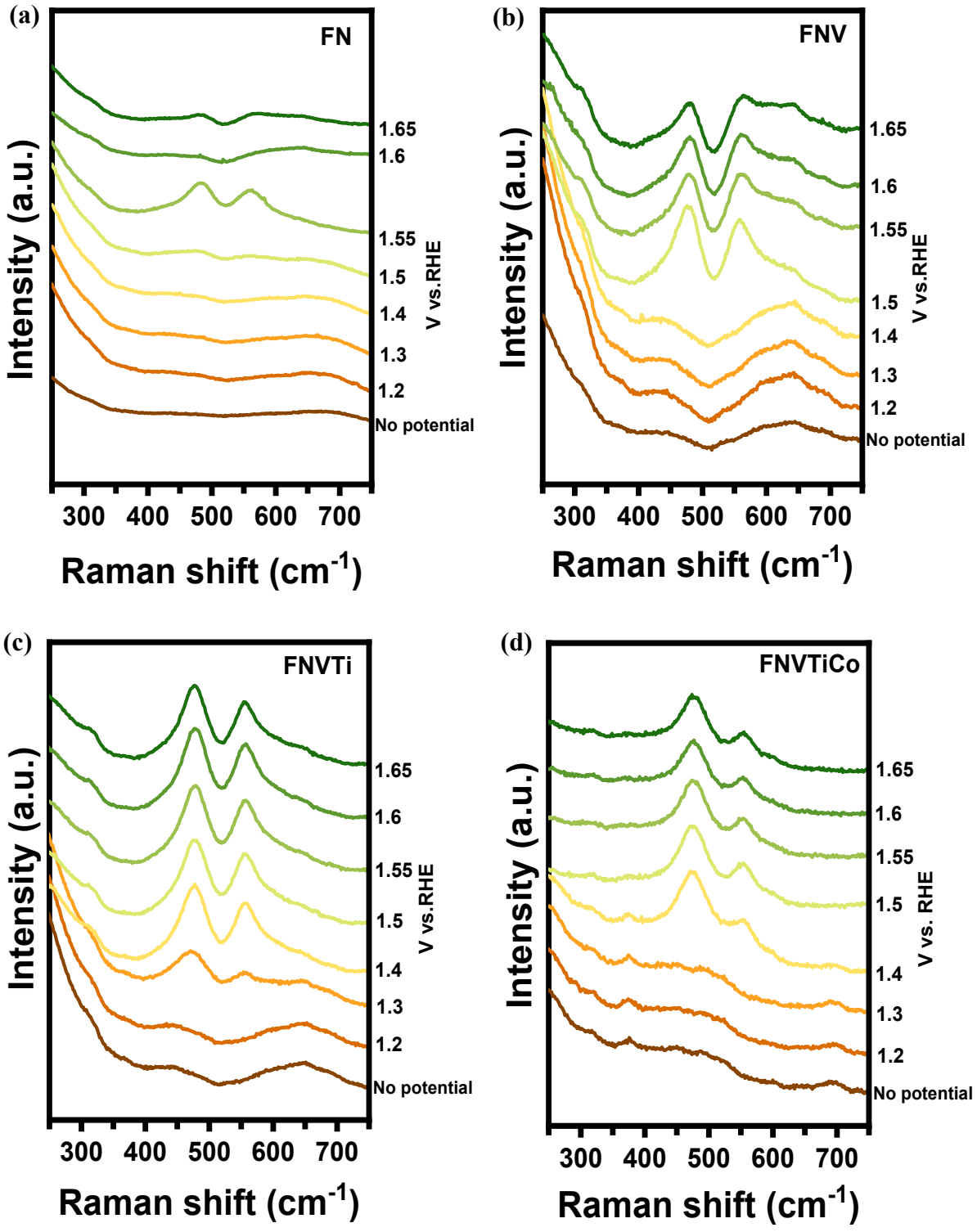

Figure S10. *In-situ* Raman spectra of hydroxides. (a) FN, (b) FNV, (c) FNVTi, and (d) FNVTiCo.

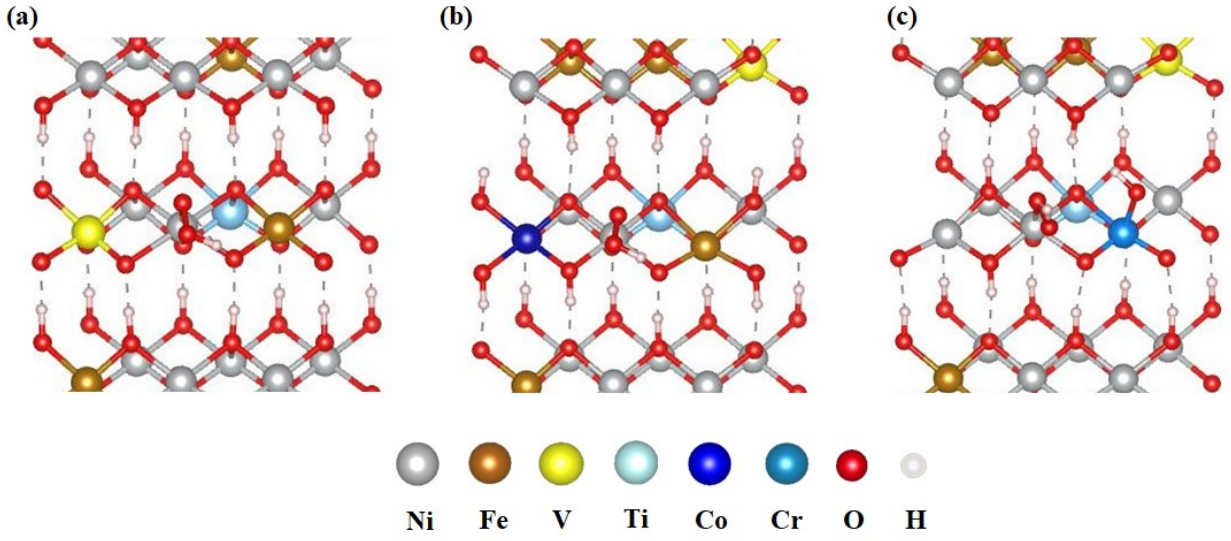

Figure S11. The top-view of optimized structure of hydroxide containing *OOH intermediates: (a) FNVTi, (b) FNVTiCo, and (c) FNVTiCr.

Information SIV. Determination of the rate determining step (RDS).

The energy change (ΔE) of each OER step in FNVTi, FNVTiCo, and FNVTiCr was calculated to determine the RDS. The RDS is the one having the highest reaction energy during OER. It is seen that from Figure SIII and Table S6 that step 4 is the RDS.

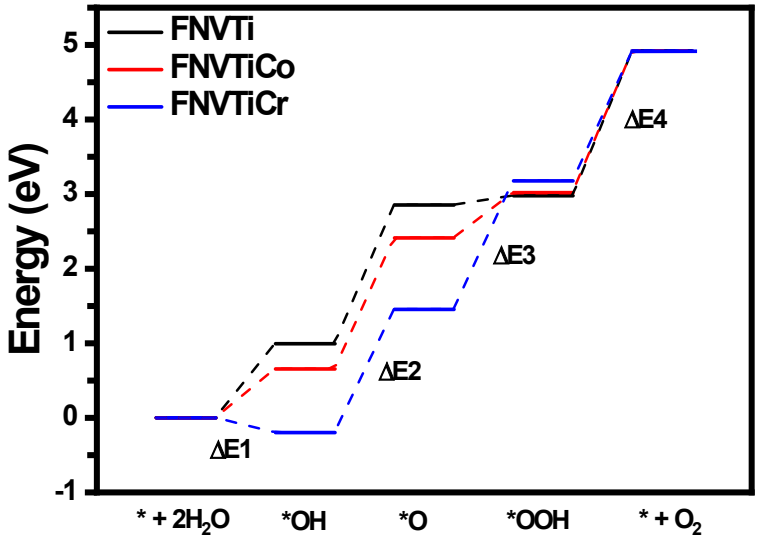

Figure SIII. OER cumulative energy diagram for the four reaction steps in OER.

Table S6. The ΔE (eV) of the four reaction steps in OER.

OER reactions	FNVTi	FNVTiCo	FNVTiCr
Step 1: $OH^- + * \rightarrow *OH + e^-$	0.99	0.66	-0.20
Step 2: $OH^- + *OH \rightarrow *O + H_2(l) + e^-$	1.86	1.75	1.65
Step 3: $OH^- + *O \rightarrow *OOH + e^-$	0.13	0.61	1.73
Step 4: $OH^- + *OOH \rightarrow *O_2(g) + H_2O + e^-$	1.94	1.90	1.74

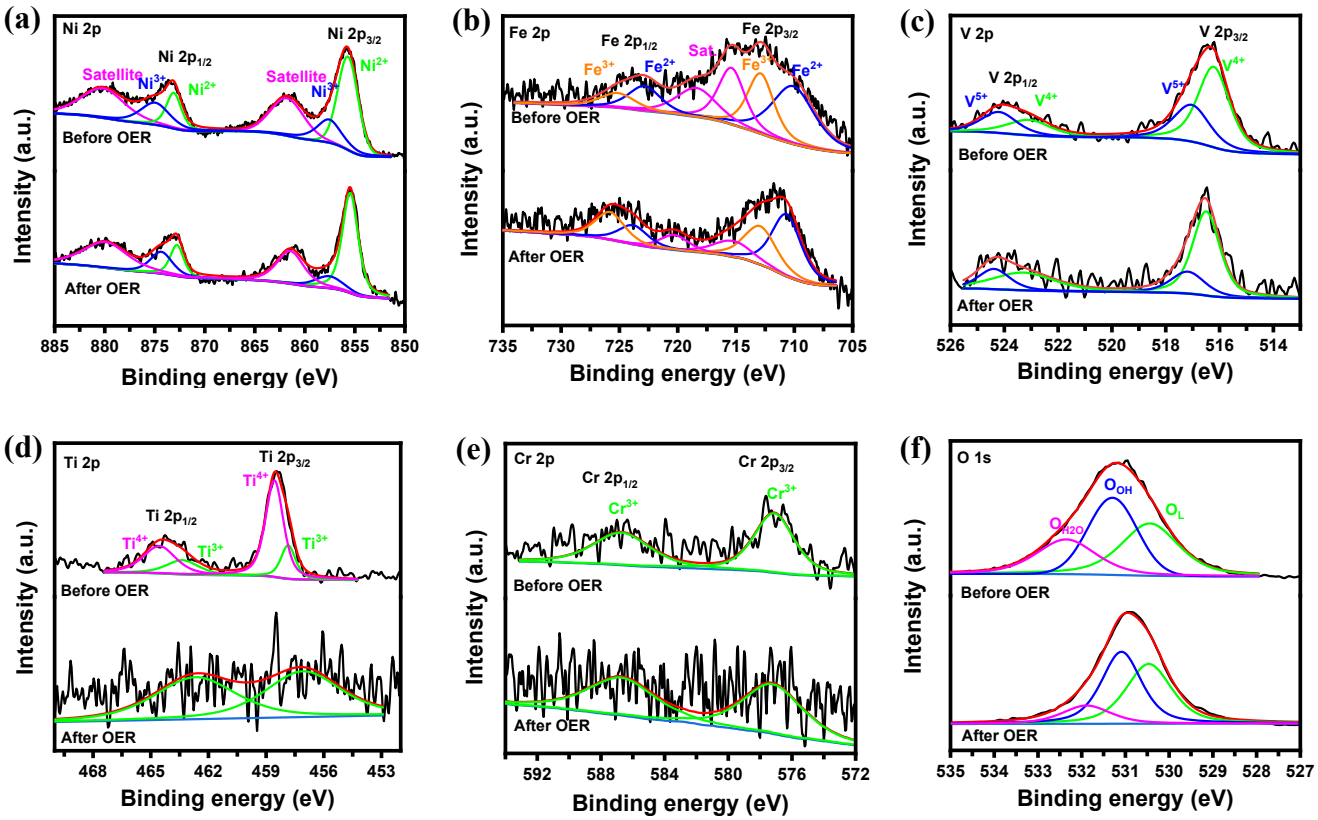

Figure S12. High resolution XPS spectra of FNVTiCr before and after OER. (a) Ni 2p, (b) Fe 2p, (c) V 2p, (d) Ti 2p, (e) Cr 2p, and (f) O 1s.

Table S7. Comparison of the overall water splitting Pt/C//FNVCrTi hydroxide cell and other reported electrolyzer have Pt/C cathode.

Cathode//Anode Catalyst	V_{10} (V)	Stability (h)	Refs.
Pt/C//FNVTiCr hydroxide	1.49	100	This work
Pt/C-$Fe_{0.4}Ni_{0.6}$ alloy//$Fe_{0.4}Ni_{0.6}$ alloy	1.50	30	[11]
Pt/C//F(V)OOH-1.5	1.51	25	[20]
Pt/C//Ni_3S_4	1.51	30	[21]
Pt/C /FeCoNi	1.52	30	[22]
Pt/C//(Ni,Fe)S_2/NiFe-CNFs	1.54	48	[23]
Pt mesh//FeNi-NFF	1.54	-	[24]
Pt/C//FeNiS	1.54	16	[25]
Pt-C//$CoFe_2O_4$	1.56	17	[26]
Pt/C// core–shell Co@NC	1.59	350	[27]
Pt foil//N-NPO/CC	1.6	2.8	[28]

References

1. Y. Liang, Y. Li, H. Wang, J. Zhou, J. Wang, T. Regier and H. Dai, *Nat. Mater.*, 2011, **10**, 780-786.
2. A. R. Jadhav, A. Kumar, J. Lee, T. Yang, S. Na, J. Lee, Y. Luo, X. Liu, Y. Hwang, Y. Liu and H. Lee, *J. Mater. Chem. A*, 2020, **8**, 24501-24514.
3. S. Hao, L. Chen, C. Yu, B. Yang, Z. Li, Y. Hou, L. Lei and X. Zhang, *ACS Energy Lett.*, 2019, **4**, 952-959.
4. X. Li, C. Liu, Z. Fang, L. Xu, C. Lu and W. Hou, *Small*, 2022, **18**, 2104354.
5. L. Hu, X. Zeng, X. Wei, H. Wang, Y. Wu, W. Gu, L. Shi and C. Zhu, *Appl. Catal. B Environ.*, 2020, **273**, 119014.
6. Z. Liu, B. Tang, X. Gu, H. Liu and L. Feng, *Chem. Eng. J.*, 2020, **395**, 125170.
7. H. Khani, N. S. Grundish, D. O. Wipf and J. B. Goodenough, *Adv. Energy Mater.*, 2020, **10**, 1903215.
8. C. Wang, H. Yang, Y. Zhang and Q. Wang, *Angew. Chem. Int. Ed.*, 2019, **58**, 6099-6103.
9. C. Liang, P. Zou, A. Nairan, Y. Zhang, J. Liu, K. Liu, S. Hu, F. Kang, H. J. Fan and C. Yang, *Energy Environ. Sci.*, 2020, **13**, 86-95.
10. Q. Xu, H. Jiang, X. Duan, Z. Jiang, Y. Hu, S. W. Boettcher, W. Zhang, S. Guo and C. Li, *Nano Lett.*, 2021, **21**, 492-499.
11. G. Zhang, J. Zeng, J. Yin, C. Zuo, P. Wen, H. Chen and Y. Qiu, *Appl. Catal. B Environ.*, 2021, **286**, 119902.
12. L. Bai, S. Lee and X. Hu, *Angew. Chem. Int. Ed.*, 2021, **60**, 3095-3103.

13. B. Wang, K. Zhao, Z. Yu, C. Sun, Z. Wang, N. Feng, L. Mai, Y. Wang and Y. Xia, *Energy Environ. Sci.*, 2020, **13**, 2200-2208.

14. Y. Jin, S. Huang, X. Yue, H. Du and P. K. Shen, *ACS Catal.*, 2018, **8**, 2359-2363.

15. T. X. Nguyen, Y.-H. Su, C.-C. Lin, J. Ruan and J.-M. Ting, *Adv. Sci.*, 2021, **8**, 2002446.

16. T. X. Nguyen, Y.-H. Su, C.-C. Lin and J.-M. Ting, *Adv. Funct. Mater.*, 2021, **31**, 2106229.

17. N.-H. Ting, T. X. Nguyen, C.-H. Lee, Y.-C. Chen, C.-H. Yeh, H.-Y. T. Chen and J.-M. Ting, *Appl. Mater. Today*, 2022, **27**, 101398.

18. T. X. Nguyen, Z.-T. Huang and J.-M. Ting, *Appl. Surf. Sci.*, 2021, **570**, 151160.

19. L. He, N. Wang, B. Sun, L. Zhong, M. Yao, W. Hu and S. Komarneni, *J. Clean. Prod.*, 2022, **356**, 131680.

20. F. N. I. Sari, H.-S. Chen, A. k. Anbalagan, Y.-J. Huang, S.-C. Haw, J.-M. Chen, C.-H. Lee, Y.-H. Su and J.-M. Ting, *Chem. Eng. J.*, 2022, **438**, 135515.

21. K. Wan, J. Luo, C. Zhou, T. Zhang, J. Arbiol, X. Lu, B.-W. Mao, X. Zhang and J. Fransaer, *Adv. Funct. Mater.*, 2019, **29**, 1900315.

22. S. Yan, M. Zhong, C. Wang and X. Lu, *Chem. Eng. J.*, 2022, **430**, 132955.

23. M. Zhong, N. Song, C. Li, C. Wang, W. Chen and X. Lu, *J. Colloid Interface Sci.*, 2022, **614**, 556-565.

24. C. Cao, D.-D. Ma, Q. Xu, X.-T. Wu and Q.-L. Zhu, *Adv. Funct. Mater.*, 2019, **29**, 1807418.

25. C. Zhao, C. Zhang, S. Bhoyate, P. K. Kahol, N. Kostoglou, C. Mitterer, S. Hinder, M. Baker, G. Constantinides, K. Polychronopoulou, C. Rebholz and R. K. Gupta, *Catalysts*, 2019, **9**, 597.

26. C. Zhang, S. Bhoyate, C. Zhao, P. K. Kahol, N. Kostoglou, C. Mitterer, S. J. Hinder, M. A. Baker, G. Constantinides, K. Polychronopoulou, C. Rebholz and R. K. Gupta, *Catalysts*, 2019, **9**, 176.

27. A. Sivanantham, P. Ganesan, L. Estevez, B. P. McGrail, R. K. Motkuri and S. Shanmugam, *Adv. Energy Mater.*, 2018, **8**, 1702838.

28. J. Huang, Y. Sun, Y. Zhang, G. Zou, C. Yan, S. Cong, T. Lei, X. Dai, J. Guo, R. Lu, Y. Li and J. Xiong, *Adv. Mater.*, 2018, **30**, 1705045.